PERGAMON

International Journal of Rock Mechanics and Mining Sciences 36 (1999) 949–970

International Journal of Rock Mechanics and Mining Sciences

www.elsevier.com/locate/ijrmms

Modeling the effect of water, excavation sequence and rock reinforcement with discontinuous deformation analysis

Yong-Il Kim[a, b], B. Amadei[b,*], E. Pan[b]

[a]Daewoo Institute of Construction Technology, Suwon, Kyunggi-do, 440-210, South Korea
[b]Department of Civil, Environmental and Architectural Engineering, University of Colorado, Campus Box 428, Boulder, CO 80309-0428, USA

Accepted 22 May 1999

Abstract

A powerful numerical method that can be used for modeling rock-structure interaction is the discontinuous deformation analysis (DDA) method developed by Shi in 1988. In this method, rock masses are treated as systems of finite and deformable blocks. Large rock mass deformations and block movements are allowed. Although various extensions of the DDA method have been proposed in the literature, the method is not capable of modeling water-block interaction, sequential loading or unloading and rock reinforcement; three features that are needed when modeling surface or underground excavation in fractured rock. This paper presents three new extensions to the DDA method. The extensions consist of hydro-mechanical coupling between rock blocks and steady water flow in fractures, sequential loading or unloading, and rock reinforcement by rockbolts, shotcrete or concrete lining. Examples of application of the DDA method with the new extensions are presented. Simulations of the underground excavation of the 'Unju Tunnel' in Korea were carried out to evaluate the influence of fracture flow, excavation sequence and reinforcement on the tunnel stability. The results of the present study indicate that fracture flow and improper selection of excavation sequence could have a destabilizing effect on the tunnel stability. On the other hand, reinforcement by rockbolts and shotcrete can stabilize the tunnel. It is found that, in general, the DDA program with the three new extensions can now be used as a practical tool in the design of underground structures. In particular, phases of construction (excavation, reinforcement) can now be simulated more realistically. However, the method is limited to solving two-dimensional problems.

Keywords: Discontinuous deformation analysis; Blocky rock masses; Hydro-mechanical coupling; Excavation sequence; Rock reinforcement; Rockbolts; Shotcrete; Tunnel stability; Construction phases

1. Introduction

Several numerical methods are used in rock mechanics to model the response of rock masses to loading and unloading. These methods include the finite element method (FEM), the boundary element method (BEM) and the discrete element method (DEM). Compared to the FEM and BEM methods, the DEM method is tailored for structurally controlled stability problems in which there are many material discontinuities and blocks. The DEM method allows for large deformations along discontinuities and can reproduce rock block translation and rotation quite well.

The discontinuous deformation analysis (DDA) method is a recently developed technique that can be classified as a DEM method. Shi [1] first proposed the DDA method in his doctoral thesis; computer programs based on the method were developed and some applications were presented in the thesis and various publications [2–5]. Various modifications to the original DDA formulation have been reported in the rock mechanics literature, in particular, in the proceedings of the First International Forum on DDA [6] and of the 2nd International Conference on Analysis of Discontinuous Deformation [7].

* Corresponding author. Tel.: +1-303-492-7315; fax: +1-303-492-7317.
E-mail address: amadei@spot.colorado.edu (B. Amadei).

1365-1609/99/$ - see front matter
PII: S0148-9062(99)00046-7

In his doctoral thesis, Lin [8] improved the original DDA program of Shi [1] by including four major extensions: improvement of block contact, calculation of stress distributions within blocks using subblocks, block fracturing, and viscoelastic behavior. Despite these improvements, the DDA method still suffers from several major limitations when used to model the interaction of engineering structures such as concrete dams and tunnels with fractured rock masses. In this paper, three limitations are addressed: hydro-mechanical coupling, sequential loading or unloading, and rock reinforcement.

In rock masses, there are generally many discontinuities that are preferred pathways for groundwater. Water flow induces hydrostatic pressure and seepage forces that affect the state of stress in the rock masses. At the same time, changes in the state of stress induce rock mass deformation, which result in changes in the rock mass hydraulic properties. This hydro-mechanical coupling is critical and cannot be ignored when modeling rock-structure interaction in engineering problems where water is present.

As discussed more extensively by Szechy [9], the arrangement of underground openings and their excavation sequence depend on the necessary operations to be conducted in them (excavation method, installation and construction of temporary and permanent support, short-term and long-term use, etc.), the nature of the rock mass, and the rock pressure conditions encountered. Therefore, there is a practical need to simulate the different phases of underground construction and, if possible, find the optimal construction procedure considering not only rock mechanics issues but also construction time and cost.

At the outset, this paper reviews some of the basic concepts of the DDA method. Then, it presents three two-dimensional extensions that have been implemented into the original DDA program of Shi [1] and modified by Lin [8] in 1995. First, seepage is allowed to take place in the fracture space between rock blocks; flow is assumed to be steady laminar or turbulent. The hydro-mechanical coupling across rock fracture surfaces is also taken into account. The program computes water pressure and seepage throughout the rock mass of interest. Second, the program allows for sequential loading or unloading and therefore can be used to simulate construction sequence. When block elements are removed (excavation) or added (loading), the algorithm modifies the initial block elements and the initial stress data. The new data are then used as input data for the next construction step. Finally, different types of rock reinforcement (shotcrete, rockbolts, concrete lining) can be selected in the program. The shotcrete or concrete lining algorithm creates lining elements along the excavated rock surface of an underground opening with specified thickness and material properties. The rockbolt algorithm suggested by Shi [1] was modified to be applicable to the cases of sequential excavation and reinforcement, in which axial forces of rockbolts at a previous step are applied to the rockbolts as preloading in the next step. The DDA program with the three new extensions can now be used as a practical tool in the design of underground structures. In particular, phases of construction (excavation, reinforcement) can now be simulated using this new program.

2. Modeling blocky rock masses using DDA

In the DDA method, the formation of blocks is very similar to the definition of a finite element mesh. A finite element type of problem is solved in which all the elements are physically isolated blocks bounded by preexisting discontinuities. The elements or blocks used by the DDA method can be of any convex or concave shape whereas the FEM method uses only elements with predetermined topologies. When blocks are in contact, Coulomb's law applies to the contact interfaces, and the simultaneous equilibrium equations are selected and solved at each loading or time increment. The large displacements and deformations are the accumulation of small displacements and deformations at each time step. Within each time step, the displacements of all points are small, hence the displacements can be reasonably represented by first order approximations.

In general, the DDA method has a number of features similar to the FEM. For instance, the DDA and FEM methods minimize the total potential energy of a system (of blocks or elements) to establish the equilibrium equations; the displacements are the unknowns of those simultaneous equations. Also, both methods add stiffness, mass and loading submatrices to the coefficient matrix of the simultaneous equations. Finally, the DDA method use of displacement locking of contacting blocks resembles in many ways the method of adding bar elements to element contacts in the FEM. The main attraction of the DDA method is its capability of reproducing large deformations along discontinuities and large block movement; two features that are restricted with the FEM.

2.1. Block deformations

By adopting first order displacement approximations, the DDA method assumes that each block has constant stresses and strains throughout. The displacements (u, v) at any point (x, y) in a block, i, can be related in two dimensions to six displacement variables

$$\mathbf{D}_i = (d_{1i}\ \ d_{2i}\ \ d_{3i}\ \ d_{4i}\ \ d_{5i}\ \ d_{6i})^{\mathrm{T}} = (u_0\ \ v_0\ \ r_0\ \ \varepsilon_x\ \ \varepsilon_y\ \ \gamma_{xy})^{\mathrm{T}}, \tag{1}$$

where (u_0, v_0) is the rigid body translation at a specific point (x_0, y_0) within the block, r_0 is the rotation angle of the block with the rotation center at (x_0, y_0) and ε_x, ε_y and γ_{xy} are the normal and shear strains in the block. As shown by Shi [1], the complete first order approximation of block displacements takes the following form

$$\begin{bmatrix} u \\ v \end{bmatrix} = \mathbf{T}_i \mathbf{D}_i, \tag{2}$$

where

$$\mathbf{T}_i = \begin{bmatrix} 1 & 0 & -(y-y_0) & (x-x_0) & 0 & (y-y_0)/2 \\ 0 & 1 & (x-x_0) & 0 & (y-y_0) & (x-x_0)/2 \end{bmatrix} \tag{3}$$

This equation enables the calculation of the displacements (u, v) at any point (x, y) within the block (in particular, at the corners), when the displacements are given at the center of rotation and when the strains (constant within the block) are known. In the two-dimensional formulation of the DDA method, the center of rotation with coordinates (x_0, y_0) coincides with the block centroid.

2.2. Simultaneous equilibrium equations

In the DDA method, individual blocks form a system of blocks through contacts among blocks and displacement constraints on single blocks. Assuming that n blocks are defined in the block system, Shi [1] showed that the simultaneous equilibrium equations can be written in matrix form as follows

$$\begin{bmatrix} \mathbf{K_{11}} & \mathbf{K_{12}} & \mathbf{K_{13}} & \cdots & \mathbf{K_{1n}} \\ \mathbf{K_{21}} & \mathbf{K_{22}} & \mathbf{K_{23}} & \cdots & \mathbf{K_{2n}} \\ \mathbf{K_{31}} & \mathbf{K_{32}} & \mathbf{K_{33}} & \cdots & \mathbf{K_{3n}} \\ \vdots & \vdots & \vdots & \ddots & \vdots \\ \mathbf{K_{n1}} & \mathbf{K_{n2}} & \mathbf{K_{n3}} & \cdots & \mathbf{K_{nn}} \end{bmatrix} \begin{Bmatrix} \mathbf{D_1} \\ \mathbf{D_2} \\ \mathbf{D_3} \\ \vdots \\ \mathbf{D_n} \end{Bmatrix} = \begin{Bmatrix} \mathbf{F_1} \\ \mathbf{F_2} \\ \mathbf{F_3} \\ \vdots \\ \mathbf{F_n} \end{Bmatrix}, \tag{4}$$

where each coefficient $\mathbf{K}_{ij}$ is defined by the contacts between blocks i and j. Since each block i has six degrees of freedom defined by the components of $\mathbf{D_i}$ in Eq. (1), each $\mathbf{K}_{ij}$ in Eq. (4) is itself a 6×6 submatrix. Also, each $\mathbf{F}_i$ is a 6×1 submatrix that represents the loading on block i. Eq. (4) can also be expressed in a more compact form as $\mathbf{KD} = \mathbf{F}$ where $\mathbf{K}$ is a $6n \times 6n$ stiffness matrix and $\mathbf{D}$ and $\mathbf{F}$ are $6n \times 1$ displacement and force matrices, respectively. In total, the number of displacement unknowns is the sum of the degrees of freedom of all the blocks. It is noteworthy that the system of Eq. (4) is similar in form to that in finite element problems.

The solution to the system of Eq. (4) is constrained by a system of inequalities associated with block kinematics (e.g. no penetration and no tension between blocks) and Coulomb friction for sliding along block interfaces. The system of Eq. (4) is solved for the displacement variables. The final solution to that system is obtained as follows. First, the solution is checked to see how well the constraints are satisfied. If tension or penetration is found along any contact, the constraints are adjusted by selecting new locks and constraining positions and a modified version of $\mathbf{K}$ and $\mathbf{F}$ are formed from which a new solution is obtained. This process is repeated until no tension and no penetration is found along all of the block contacts. Hence, the final displacement variables for a given time step are actually obtained by an iterative process.

The simultaneous Eq. (4) were derived by Shi [1] by minimizing the total potential energy Π of the block system. The i-th row of Eq. (4) consists of six linear equations

$$\frac{\partial \Pi}{\partial d_{ri}} = 0, \quad r = 1\text{–}6, \tag{5}$$

where the d_{ri} are the deformation variables of block i. The total potential energy Π is the summation over all the potential energy sources, i.e. individual stresses and forces. The potential energy of each force or stress and their derivatives are computed separately. The derivatives

$$\frac{\partial^2 \Pi}{\partial d_{ri} \partial d_{sj}}, \quad r, s = 1\text{–}6 \tag{6}$$

are the coefficients of the unknowns d_{sj} of the equilibrium Eq. (4) for variable d_{ri}. All terms of Eq. (6) form a 6×6 submatrix, which is the submatrix $\mathbf{K}_{ij}$ in the global Eq. (4). Eq. (6) implies that matrix $\mathbf{K}$ in Eq. (4) is symmetric. The derivatives

$$-\frac{\partial \Pi(0)}{\partial d_{ri}}, \quad r = 1\text{–}6 \tag{7}$$

are the free terms of Eq. (5) which are shifted to the right hand side of Eq. (4). All these terms form a 6×1 submatrix, which is added to the submatrix $\mathbf{F}_i$.

Shi's thesis [1] covers the details for forming submatrices $\mathbf{K}_{ij}$ and $\mathbf{F}_i$, for elastic stresses, initial stresses, point loads, line loads, volume forces, bolting forces, inertia forces and viscosity forces. Both static and dynamic analyses can be conducted with the DDA method. For static analysis, the velocity of each block in the blocky system at the beginning of each time step is assumed to be zero. On the other hand, in the case

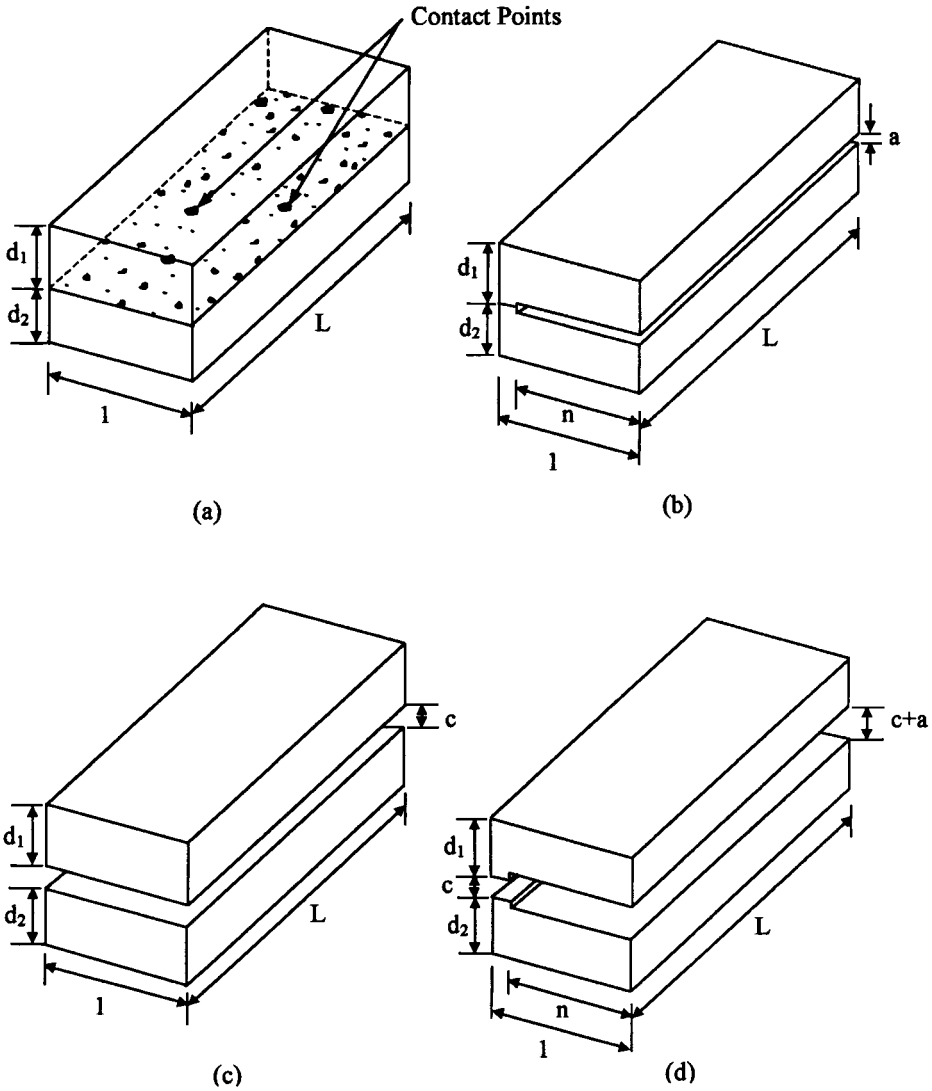

Fig. 1. Joint modeling. (a) Representative section of closed joint, (b) Idealized section of closed joint, (c) Representative section of open joint, (d) Idealized section of open joint.

of dynamic analysis, the velocity of the blocky system in the current time step is an accumulation of the velocities in the previous time steps.

3. Modeling water-block interaction in DDA

A numerical model was developed to study fluid flow in deformable naturally fractured rock masses. The model considers a two-dimensional intact rock mass dissected by a large number of fractures (joints) with variable aperture, length, and orientation. Fluid flow, which occurs when pressure gradients exist, is assumed to be steady, and laminar or turbulent depending on the values of the Reynolds number and the relative roughness of the fracture walls [10]. Fluid flow and the rock deformation are fully coupled. Variations in fluid pressure and quantity of fluid result in joint deformation. In turn, joint deformation changes the joint properties, which therefore changes the fluid pressures and the resistance to fluid flow.

3.1. Assumptions

The following assumptions were made when implementing the hydro-mechanical coupling in the DDA program: (a) the fluid is incompressible, (b) the intact rock is impervious, and fluid flow takes place in the joint space only; (c) the rock mass contains a finite number of joints; (d) the intact rock is linearly elastic; and (e) joint displacements are small relative to the joint dimensions.

In the flow model, the fracture space is idealized as a system of one-dimensional conduits of constant aper-

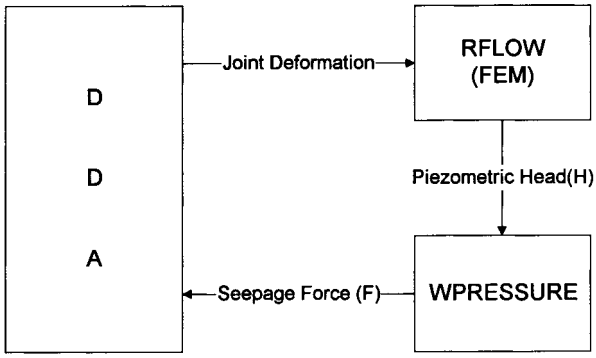

Fig. 2. Water-block interaction model.

ture using the approach proposed by Asgian [11]. The *apparent* aperture, b, of a conduit representing a joint depends on the contact between the joint surfaces. The joint can be classified as closed or open depending on the contact state. Consider, for instance, a closed joint with length, L, and unit width representing the interface between two contacting prismatic blocks of thickness d_1 and d_2 as shown in Fig. 1(a). Let n be the joint surface *contact porosity* (ratio between joint surface open area and total area) of the closed joint which varies between 0 and 1. The joint can be idealized as a portion of void (n) with a uniform aperture, a, and a portion of contacting solid ($1-n$) with vanishing aperture as shown in Fig. 1(b). The *apparent* aperture, b, of the closed joint is defined as $b=a$ for the portion of void (n).

A representative section of an open joint with length, L, and unit width is shown in Fig. 1(c). The joint represents the open interface between two prismatic blocks of thickness d_1 and d_2 separated by a gap c. The joint can be idealized as one portion of void (n) with aperture, $c+a$, and another portion of void ($1-n$) with aperture, c, as shown in Fig. 1(d). The *apparent* aperture, b, of the open joint consists of two components with $b_n=c+a$ for the portion of void (n) and $b_{1-n}=c$ for the other portion of void ($1-n$).

3.2. Configuration of water-block interaction model

As shown in Fig. 2, the hydro-mechanical model consists of two major components: the DDA method for the rock mass and the FEM method for joint flow. The initial properties of the joints such as aperture, length, orientation, and boundary conditions from the DDA program are used to compute the piezometric heads and fluid quantities at the joints with a FEM subroutine called RFLOW. The seepage forces acting on the rock blocks are computed from the piezometric heads using a subroutine called WPRESSURE. In the DDA program, joint deformation is computed using the seepage forces. In turn, joint deformation changes the joint properties such as aperture, length, and orientation. A computational loop is followed until the

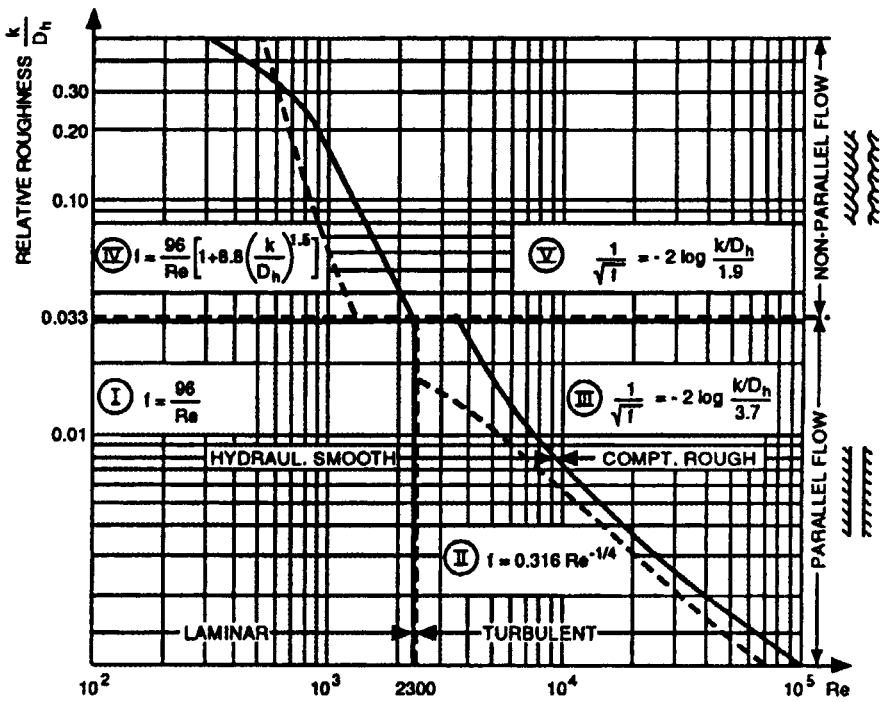

Fig. 3. Compilation of different flow laws and their range of validity for a single fracture. The dashed lines represent mathematical boundaries by Amadei et al. [12] and the solid lines the boundaries determined experimentally by Louis [10].

Table 1
Expression of hydraulic conductivity and degree of nonlinearity for the different hydraulic regions of Fig. 3 (after Louis [10])

Hydraulic region	Hydraulic conductivity (K)	Exponent (α)	Flow condition
I	$K_{\mathrm{I}} = gb^2/12\nu$	1.0	laminar
II	$K_{\mathrm{II}}=(1/b)[(g/0.079)(2/\nu)^{0.25} \times b^3]^{4/7}$	4/7	turbulent
III	$K_{\mathrm{III}} = 4\sqrt{g}\log[3.7/(k/D_{\mathrm{h}})]\sqrt{b}$	0.5	turbulent
IV	$K_{\mathrm{IV}} = [gb^2]/(12\nu[1 + 8.8(k/D_{\mathrm{h}})^{1.5}])$	1.0	laminar
V	$K_{\mathrm{V}} = 4\sqrt{g}\log[1.9/(k/D_{\mathrm{h}})]\sqrt{b}$	0.5	turbulent

results converge according to a criterion selected by the user.

3.3. Subroutine RFLOW

Louis [10] showed experimentally that the steady flow of water in a single fracture of constant aperture, b, and surface roughness can be laminar or turbulent depending on the values of the Reynolds number, $Re = 2b\upsilon/\nu$, and the relative roughness, k/D_h, where υ is the average velocity, ν the kinematic viscosity of water, k the fracture surface roughness, and D_{h} the hydraulic diameter of the fracture which is equal to $2b$. Louis [10] also proposed different flow laws relating the friction factor f and the Reynolds number Re which apply in different regions of the (Re, k/D_{h}) space. Fig. 3 shows five such regions I–V, their corresponding mathematical boundaries and the experimental boundaries proposed by Louis [10].

For parallel flow, and as shown by Amadei et al. [12], the mathematical boundary between turbulent hydraulic smooth flow (region II) and turbulent completely rough flow (III) in Fig. 3 can be expressed as

$$Re = 2.553\left[\log\left(\frac{k/D_{\mathrm{h}}}{3.7}\right)\right]^8 \tag{8}$$

For non-parallel flow, and as shown by Amadei et al. [12], the mathematical boundary between laminar flow (region IV) and turbulent flow (region V) in Fig. 3 can be expressed as

$$Re = 384\left[1 + 8.8(k/D_{\mathrm{h}})^{1.5}\right]\left[\log\left(\frac{k/D_h}{1.9}\right)\right]^2 \tag{9}$$

The mathematical boundaries defined by Eqs. (8) and (9) are shown as dashed lines in Fig. 3. These mathematical boundaries were used in the nonlinear model presented below.

According to Bernoulli's theorem for ideal frictionless incompressible fluids, the sum of the *pressure head*, $h_{\mathrm{p}} = p/\gamma_{\mathrm{w}}$, *elevation head*, $h_{\mathrm{e}} = z$, and *velocity head*, $h_{\mathrm{v}} = \upsilon^2/2g$, is constant at every point of the fluid, e.g.

$$\frac{p}{\gamma_{\mathrm{w}}} + z + \frac{\upsilon^2}{2g} = H + h_v = \text{constant} = H_{\mathrm{t}} \tag{10}$$

where p is the pressure, z the elevation, υ the average velocity, H the piezometric head ($= h_{\mathrm{p}} + h_{\mathrm{e}}$), and H_{t} the total head.

In the steady flow of water in a single fracture of constant aperture, b, and length, L, the total head loss, ΔH_{t}, (also equal to the piezometric head loss, $\mathbf{\Delta}H$) takes place due to the viscous resistance within the fracture. As shown by Louis [10], the average velocity, υ, and the gradient of piezometric head, $i = \mathbf{\Delta}H/L$, (also equal to the gradient of total head, $\mathbf{\Delta}H_{\mathrm{t}}/L$) for each hydraulic region of Fig. 3 can be written as follows

$$\upsilon = Ki^{\alpha} = K\left(\frac{\Delta H}{L}\right)^{\alpha} \tag{11}$$

where ΔH is the piezometric head loss. Values of the hydraulic conductivity, K, and the exponent, α, for each flow region of Fig. 3 are reported in Table 1. For each hydraulic region, the element discharge, Q, and the piezometric gradient, $i = \mathbf{\Delta}H/L$, are such that

$$Q = \upsilon b = Kb\left(\frac{\Delta H}{L}\right)^{\alpha} \tag{12}$$

Equation (12) can be rewritten as

$$Q = T\Delta H \text{ with } T = \frac{Kb}{L^{\alpha}}\Delta H^{\alpha-1} \tag{13}$$

where T is the so-called fracture transmissivity.

Equation (13) is then modified depending on the contact state (closed or open) between the joint surfaces. For a closed joint (Fig. 1(b)), the element discharge, Q, is defined as

$$Q = T\Delta H \text{ with } T = n\frac{Kb}{L^{\alpha}}\Delta H^{\alpha-1} \tag{14}$$

For an open joint (Fig. 1(d)), the element discharge, Q, is defined as

$$Q = T\Delta H \text{ with}$$

$$T = n\frac{K_n b_n}{L^{\alpha_n}}\Delta H^{\alpha_n - 1} + (1-n)\frac{K_{1-n} b_{1-n}}{L^{\alpha_{1-n}}}\Delta H^{\alpha_{1-n}-1}, \tag{15}$$

where K_n and α_n are respectively the hydraulic conduc-

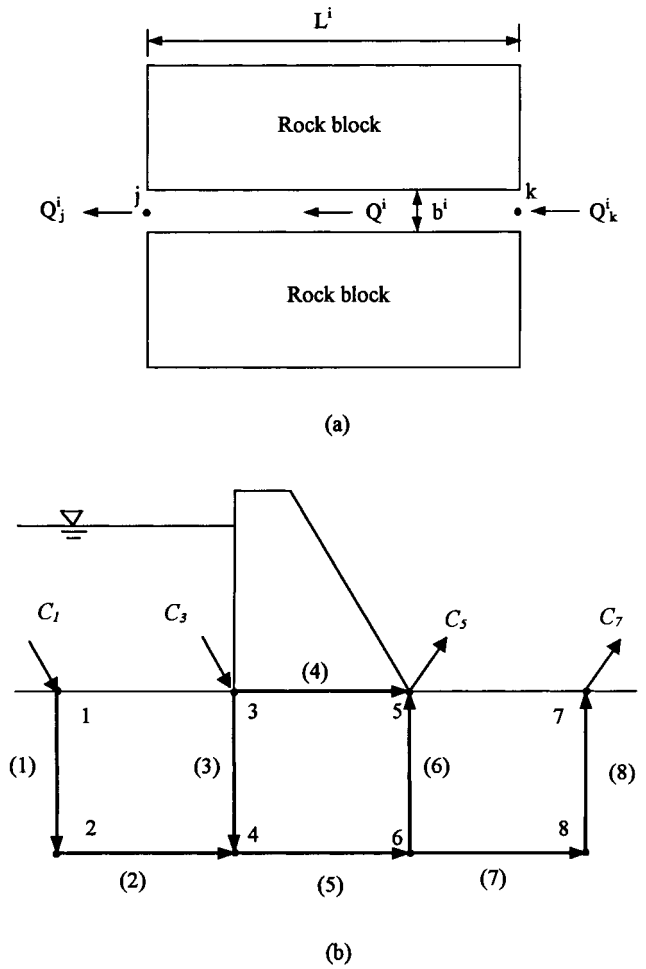

Fig. 4. Construction of total system of equations. (a) Single joint element, (b) Joint network.

tivity and exponent for one portion of void (n) with apparent aperture $b_n = c + a$. Likewise, K_{1-n} and α_{1-n} are respectively the hydraulic conductivity and exponent for the other portion of void $(1-n)$ with apparent aperture $b_{1-n} = c$.

Consider now a single planar joint element, i, of length L^i and constant aperture b^i as shown in Fig. 4(a). Eq. (13) can be used to compute the discharge through the joint element in terms of the piezometric head loss between its two end nodes defined here as j and k. The discharge at node k, Q^i_k, and the discharge at node j, Q^i_j, are equal to

$$Q^i_k = T^i \Delta H^i = T^i \left(H^i_k - H^i_j \right)$$

$$Q^i_j = -T^i \Delta H^i = -T^i \left(H^i_k - H^i_j \right) \tag{16}$$

These two equations can be rewritten in matrix form as follows:

$$\begin{Bmatrix} Q^i_k \\ Q^i_j \end{Bmatrix} = T^i \begin{bmatrix} 1 & -1 \\ -1 & 1 \end{bmatrix} \begin{Bmatrix} H^i_k \\ H^i_j \end{Bmatrix} \text{ or } \mathbf{Q}^i = \mathbf{T}^i \mathbf{H}^i, \tag{17}$$

where $\mathbf{Q}^i$ is the element nodal discharge vector, $\mathbf{T}^i$ the element characteristic matrix, and $\mathbf{H}^i$ the element nodal piezometric head vector.

So far, the elements in the network have been considered individually, and expressions giving the discharges in terms of the nodal piezometric heads have been developed. For a complete joint network, however, the interaction between the different elements needs to be taken into account. This implies that there must exist equilibrium at any given node of the network between the discharges of the elements connected to the node, including any inflow or outflow at that node. Consider a simplified model of a fracture network below a dam as shown in Fig. 4(b). The quantity C_j is the inflow (C_1 and C_3) or outflow (C_5 and C_7) at any node j. In general, any C_j will be positive for inflow (C_1 and C_3) and negative for outflow (C_5 and C_7). Equilibrium at any node means that the sum of the discharges of the elements connected to the node equals the inflow or outflow at that node. For any node j, the equilibrium equation can be expressed as follows:

$$\sum_i Q^i_j = C_j \tag{18}$$

where the summation runs over all elements connected to node j. By repeating the procedure for all n nodes, and using Eqs. (17) and (18), a system of equilibrium equations can be derived e.g.

$$\begin{bmatrix} T_{11} & T_{12} & \dots & T_{1n} \\ T_{21} & T_{22} & \dots & T_{2n} \\ \vdots & \vdots & \ddots & \vdots \\ T_{n1} & T_{n2} & \dots & T_{nn} \end{bmatrix} \begin{Bmatrix} H_1 \\ H_2 \\ \vdots \\ H_n \end{Bmatrix} = \begin{Bmatrix} C_1 \\ C_2 \\ \vdots \\ C_n \end{Bmatrix} \tag{19}$$

or $\mathbf{TH} = \mathbf{C}$

where $\mathbf{T}$ is the network characteristic matrix, $\mathbf{H}$ is the network piezometric head vector, and $\mathbf{C}$ is the network flow vector. Before the total system of Eq.(19) can be solved, it is necessary to introduce the boundary conditions for the network nodes. The boundary conditions at a given node j can be of two types; specified piezometric head (H_j) or specified flow (C_j).

The total system of Eq.(19) is a nonlinear system due to the fact that $\mathbf{T}$ depends on $\mathbf{H}$. However, it can be solved by successive iterations. First, for each joint element, flow is assumed to be laminar with $\alpha = 1.0$ and $K = K_{\mathrm{I}}$ or K_{IV} and an initial value for the nodal piezometric head, H_{ini}, is assumed for each node.The fracture transmissivity, T, is computed using Eqs. (14) or (15) for each joint element, and the total system of

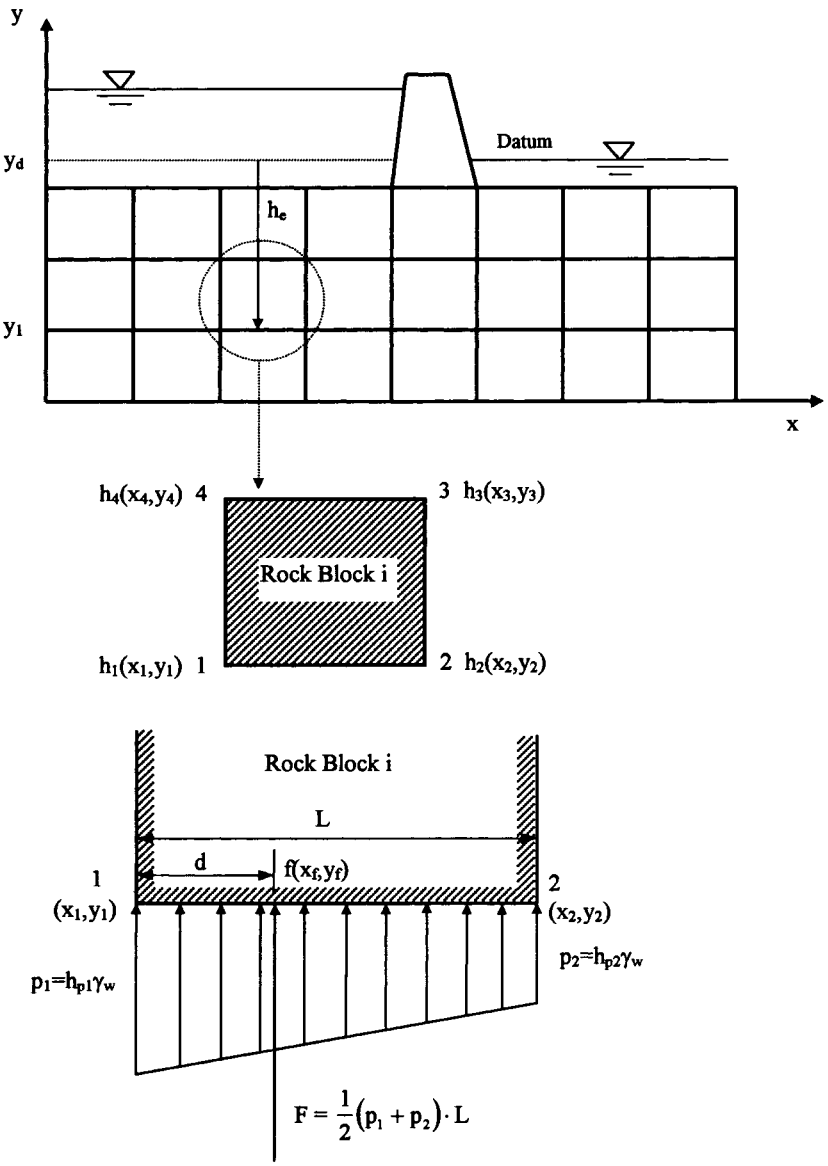

Fig. 5. Conversion of nodal head into point load.

Eq. (19) is formed using Eqs. (17) and (18). The total system of equations is solved by the Gauss elimination method to obtain a new value of the nodal piezometric head, H_{new}, for each node. The velocity, υ, defined by Eq. (11) and the Reynolds number, $Re = 2b\upsilon/\nu$, are calculated for each joint element using the new value of the nodal heads. Using Fig. 3, the values of Re and the relative roughness, k/D_h, determine if the flow in each joint element is laminar or turbulent. If the flow is laminar, α and K remain the same. If, on the other hand, turbulent flow develops, new values of α and K are selected using Fig. 3 and Table 1 for each joint element, and a new initial value for the nodal piezometric head is assumed with $H_{ini} = H_{new}$ for each node in the next iteration. Then, using Eqs. (14) or (15), a new fracture transmissivity, T, is computed for each element, and a new total system of equations is formed. The total system of equations is solved to obtain a new value of the nodal piezometric head, H_{new}, for each node. The process is repeated until, for two successive steps, α and K remain the same and $|H_{new}-H_{ini}|/H_{ini}$ is below a minimum tolerance specified by the user.

3.4. Subroutine WPRESSURE

A new algorithm for computing seepage forces acting on rock blocks from the nodal piezometric heads

was developed. The fluid pressure acting on the rock blocks can be computed from the values of the pressure heads at those nodes defining the blocks. The fluid pressures are transformed as point loads along the sides of each rock block. Then, the point loads are given as boundary conditions in the discontinuous deformation analysis. Using this approach, there is no need to artificially regulate the deformations of the joints as in other methods. Therefore, the rock blocks can deform freely according to block system kinematics.

As an example, consider flow through the joint network of Fig. 5. Subroutine RFLOW gives value of the piezometric head, H, at each node. Then, at each node, the pressure head, h_p, can be computed from H, and the elevation head, $h_e = y - y_d$, as

$$h_p = H - h_e = H - y + y_d \tag{20}$$

where y is the vertical coordinate of the node, y_d the vertical coordinate of the datum line. For rock block, i, in Fig. 5, h_p can be calculated by using Eq. (20) at nodes 1 and 2 with $h_{p1} = H_1 - y_1 + y_d$ and $h_{p2} = H_2 - y_2 + y_d$. The pressures at node 1 and 2 are then equal to $p_1 = h_{p1}\gamma_w$ and $p_2 = h_{p2}\gamma_w$, respectively. For a closed joint with a *contact porosity*, n, the total seepage force, F, acting on the edge between nodes 1 and 2 is calculated as

$$F = n\tfrac{1}{2}(p_1 + p_2) \times L \text{ with}$$

$$L = \sqrt{(x_1 - x_2)^2 + (y_1 - y_2)^2} \tag{21}$$

For an open joint, n is equal to 1.0. The distance, d, between node 1 and the loading point f (x_f, y_f) where F is applied can be calculated by moment equilibrium at point 1. When p_1 is larger than p_2 (Fig. 6(a)), d is equal to

$$d = \frac{F_1 \times L/2 + F_2 \times L/3}{F} \text{ with } F_1 = np_2L$$

$$\text{and } F_2 = n\tfrac{1}{2}(p_1 - p_2) \times L \tag{22}$$

When p_1 is smaller than p_2 (Fig. 6(b)), d is equal to

$$d = \frac{F_1 \times L/2 + F_2 \times 2L/3}{F} \text{ with } F_1 = np_1L$$

$$\text{and } F_2 = n\tfrac{1}{2}(p_2 - p_1) \times L \tag{23}$$

When p_1 is equal to p_2, $d = 1/2$. In all cases, the coordinates (x_f, y_f) of the loading point are equal to

$$x_f = x_1 + \frac{d}{L}(x_2 - x_1); \quad y_f = y_1 + \frac{d}{L}(y_2 - y_1). \tag{24}$$

In general, the horizontal and vertical components (F_x and F_y) of the total seepage force F can be calculated as follows:

- when $x_2 > x_1$ (Fig. 7(a,b)),

$$F_x = -F\sin\alpha,$$

$$F_y = F\cos\alpha \text{ with } \alpha = \tan^{-1}\left(\frac{y_2 - y_1}{x_2 - x_1}\right) \tag{25}$$

- when $x_1 > x_2$ (Fig. 7(c,d)),

$$F_x = F\sin\alpha,$$

$$F_y = -F\cos\alpha \text{ with } \alpha = \tan^{-1}\left(\frac{y_2 - y_1}{x_2 - x_1}\right) \tag{26}$$

- when $x_1 = x_2$ and $y_2 > y_1$ (Fig. 7(e)),

$$F_x = -F, \quad F_y = 0 \tag{27}$$

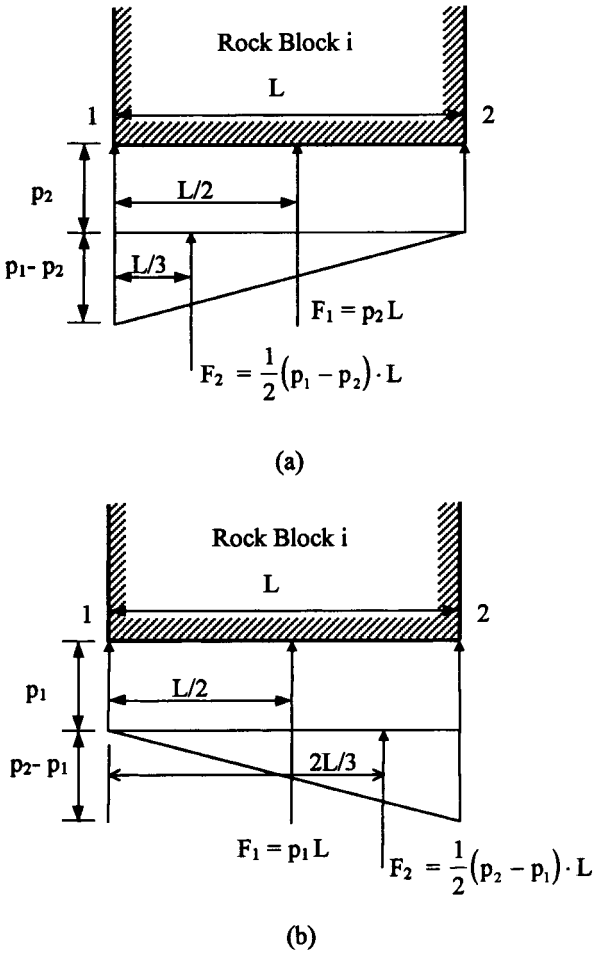

Fig. 6. Distance to the loading point. (a) $p_1 > p_2$, (b) $p_1 < p_2$.

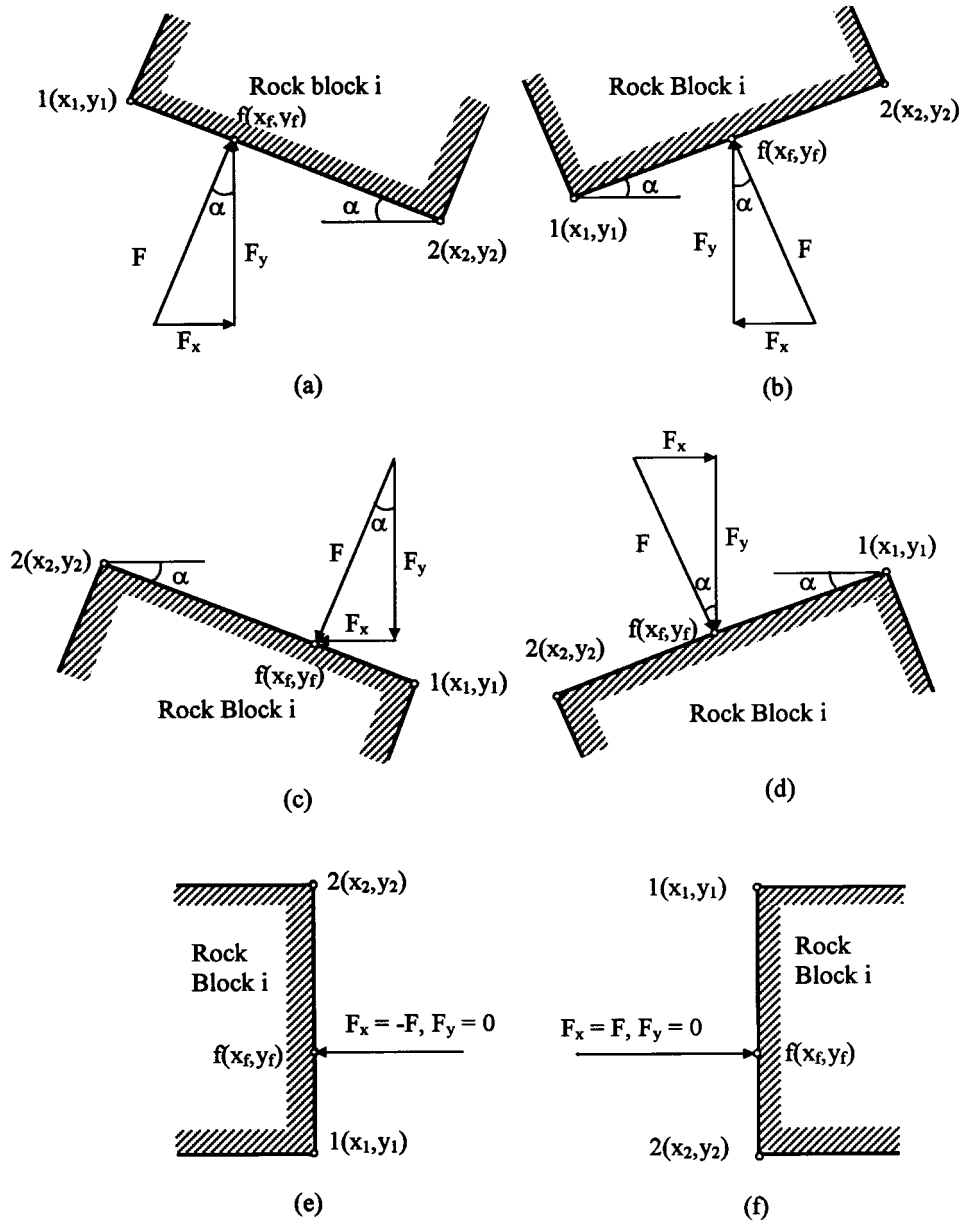

Fig. 7. Computation of F_x and F_y. (a) $x_1 < x_2$, $y_1 \geq y_2$, (b) $x_1 < x_2$, $y_1 < y_2$, (c) $x_1 > x_2$, $y_1 < y_2$, (d) $x_1 > x_2$, $y_1 \geq y_2$, (e) $x_1 = x_2$, $y_1 < y_2$, (f) $x_1 = x_2$, $y_1 > y_2$.

- when $x_1 = x_2$ and $y_1 > y_2$ (Fig. 7(f)),

$$F_x = F, \quad F_y = 0 \tag{28}$$

3.5. Application of seepage forces on rock blocks

Shi [1] derived a formulation for the components of submatrices $\mathbf{F}_i$ for the case of point loading. A seepage force can be considered as a point load acting along the edge of a rock block. The seepage force with components (F_x, F_y) acts at point (x_f, y_f) on rock block, i, as shown in Fig. 7(a,f). According to Eq. (2), the displacement components (u_f, v_f) at point (x_f, y_f) along the edge of rock block, i, are equal to

$$\begin{bmatrix} u_f \\ v_f \end{bmatrix} = \mathbf{T}_i \mathbf{D}_i = \begin{pmatrix} t_{11} & t_{12} & t_{13} & t_{14} & t_{15} & t_{16} \\ t_{21} & t_{22} & t_{23} & t_{24} & t_{25} & t_{26} \end{pmatrix} \begin{Bmatrix} d_{1i} \\ d_{2i} \\ d_{3i} \\ d_{4i} \\ d_{5i} \\ d_{6i} \end{Bmatrix} \tag{29}$$

The potential energy associated with the seepage force with components (F_x, F_y) is then equal to

$$\Pi_f = -\left(F_x u_f + F_y v_f\right) = -\begin{pmatrix} u_f & v_f \end{pmatrix}\begin{pmatrix} F_x \\ F_y \end{pmatrix}$$
$$\Pi_f = -\mathbf{D}_i^{\mathrm{T}}\mathbf{T}_i^{\mathrm{T}}\begin{pmatrix} F_x \\ F_y \end{pmatrix} \tag{30}$$

To minimize Π_f, derivatives are computed and yield

$$f_r = -\frac{\partial \Pi_f(0)}{\partial d_{ri}} = \frac{\partial}{\partial d_{ri}}\mathbf{D}_i^{\mathrm{T}}\mathbf{T}_i^{\mathrm{T}}\begin{pmatrix} F_x \\ F_y \end{pmatrix} = F_x t_{1r} + F_y t_{2r}, \quad r = 1\text{–}6 \tag{31}$$

where f_r (r = 1–6,) are the components of a 6×1 submatrix

$$\mathbf{T}_i^{\mathrm{T}}\begin{pmatrix} F_x \\ F_y \end{pmatrix} = \begin{pmatrix} t_{11} & t_{21} \\ t_{12} & t_{22} \\ t_{13} & t_{23} \\ t_{14} & t_{24} \\ t_{15} & t_{25} \\ t_{16} & t_{26} \end{pmatrix}\begin{pmatrix} F_x \\ F_y \end{pmatrix} \rightarrow \mathbf{F}_i \tag{32}$$

which is the product matrix of a 6×2 matrix (whose components are defined in Eq. (3)) and a 2×1 matrix. The resulting 6×1 submatrix is added to the submatrix $\mathbf{F}_i$ in the global system of Eq. (4).

3.6. Comparison with the experimental work of Grenoble [13]

As a validity check of the RFLOW subroutine, a comparison was made with the experimental work reported by Grenoble [13], who constructed a physical laboratory model to simulate two-dimensional flow through a jointed rock mass. The joint network of the model was formed by sawing 12.7 mm (0.5 inch) deep and 0.508 mm (0.02 inch) wide slots in the face of a 25.4 mm (1.0 inch) thick sheet of Plexiglas. A schematic of the complete test set-up is illustrated in Fig. 8(a) and the model joint pattern is shown in Fig. 8(b). The water pressure was measured at 24 joint intersection ports as shown in Fig. 8(b). Grenoble [13] conducted nine tests (T1-3 to T1-11) subjecting the model to hydraulic gradients ranging between 0.01 and 2.84 (resulting in a head differential across the model ranging between 0.762 cm and 172.84 cm). The test procedure consisted of applying a head differential, allowing the system to come to equilibrium, and then reading the head values at the measurement ports.

As the laboratory model was made of one plate with slots, all blocks in the DDA model were modeled as subblocks. The Plexiglas was assumed to have a unit weight of 11.7 kN/m^3, a Young's Modulus of 3.1 GPa and a Poisson's ratio of 0.35. The joints were assumed to have no friction or cohesion. The kinematic viscosity of water was taken equal to 1.005×10^{-6} m^2/sec. Six representative tests (T1-5 to T1-10) were analyzed by the DDA program containing the RFLOW subroutine (Table 2). For each test, the head values computed by the revised DDA program were compared with the values measured in the laboratory model at all measurement ports (Table 2). The error in head value, E_i, at each measurement port, i, was calculated as follows

$$E_i = \frac{h_{\mathrm{l}} - h_{\mathrm{d}}}{H - h}, \tag{33}$$

where h_{l} is the head value measured in the laboratory; h_{d} is the value predicted by the DDA program; H is the upstream head; and h is the downstream head. For each test, the average error in head value, E_{h}, for each test was calculated as

$$E_{\mathrm{h}} = \frac{1}{n}\sum_{i=1}^{n}|E_i|, \tag{34}$$

where n (n = 24) is the number of measurement ports. Values of E_{h} are reported in Table 2.

The results in Table 2 indicate that the average error does not exceed 5.83% and its magnitude increases with the hydraulic gradient. This increase is probably due to the fact that the pressure ports disturb the flow and the magnitude of the disturbance increases with the flow velocity [13].

3.7. Comparison with the analytical solution of Sneddon and Lowengrub [14]

As a validity check of the WPRESSURE subroutine in the DDA program, the problem of the opening of a crack (joint) in an infinite domain subjected to an internal pressure was considered. The geometry of the problem is shown in Fig. 9(a). An internal pressure P is applied on the walls of a crack of length, $2L$, resulting in a maximum deformation, $D_{\mathrm{n,max}}$, at the center of the crack.

Two DDA models for this problem are shown in Fig. 9(b,c). The crack length is $2L$ = 20 m and the domain of analysis is $10L \times 10L$ (100 m × 100 m). The crack has a friction angle of 45°, and no cohesion. The intact rock has a unit weight of 26.0 kN/m^3, a Young's modulus of 2.5 GPa, and a Poisson's ratio of 0.25. The fluid has a kinematic viscosity of 2.0×10^{-7} m^2/sec. At the crack ends ($x = \pm L$), the pressure heads were fixed at 22.45 m as boundary conditions, thus a constant fluid pressure of 0.22 MPa was applied on the crack wall surfaces. Two cases were considered for comparison in which the walls of the crack were

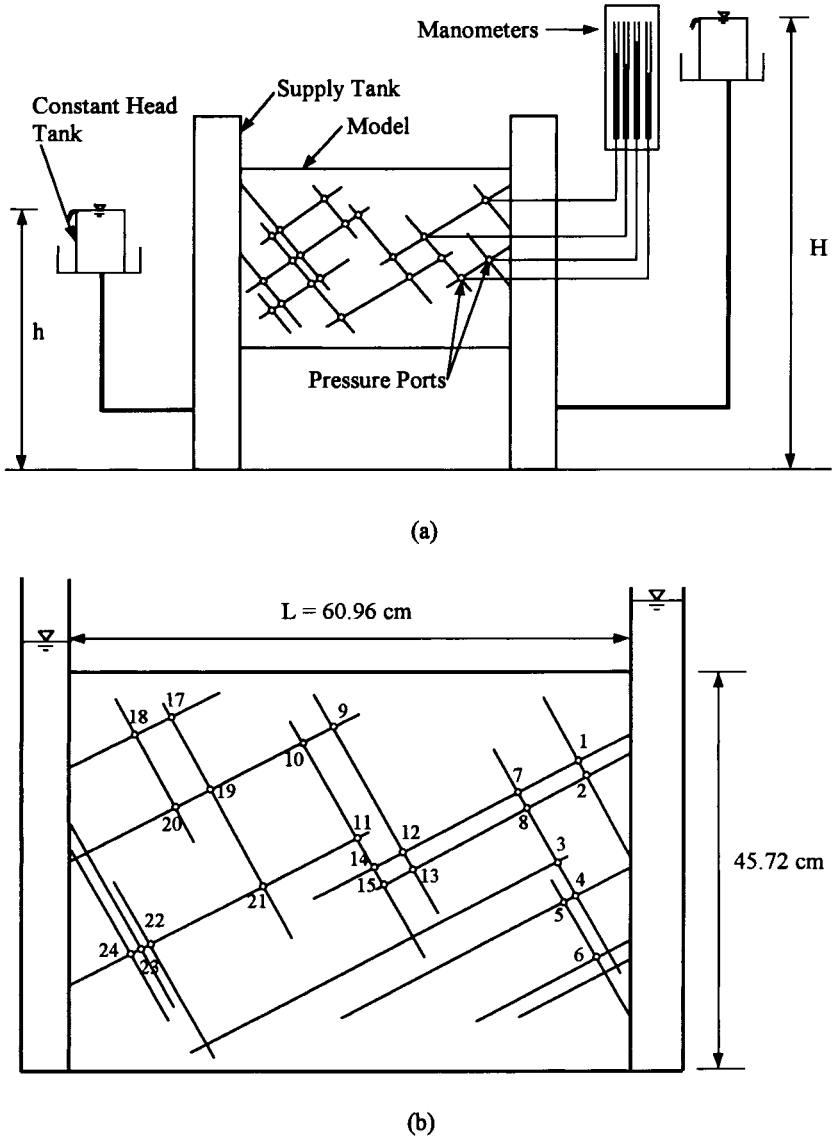

Fig. 8. Laboratory model of Grenoble [13]. (a) Schematic of the complete laboratory test set-up, (b) Layout of the joint pattern in the physical model.

divided into 6 subblocks (Fig. 9(b)) and 10 subblocks (Fig. 9(c)).

The crack opening for this problem was also computed using the analytical solution given by Sneddon and Lowengrub [14]:

$$D_n = \frac{2(1-\nu)}{G} PL\sqrt{(1-x^2/L^2)}, \tag{35}$$

where L is the crack half-length, D_n the crack opening along the interval $-L \le x \le L$, G is the shear modulus of the elastic medium; P is the pressure acting on the crack wall surfaces; x is the distance along the crack measured from the center of the crack; and ν is the Poisson's ratio.

The analytical and numerical predictions for the crack wall deformation profiles for the two cases are compared in Figs. 10(a) and 10(b). At the center of the crack, the numerical solution deviates from the analytical solution by 3.9% for the case in which 6 subblocks are used to compute the crack displacement (Fig. 10(a)). When 10 subblocks are used instead (Fig. 10(b)), the deviation of the numerical solution from the analytical solution reduces to 1.1%. At the crack ends ($x = \pm L$), the numerical solution deviates from the analytical solution by 15.8% for the 6 subblocks case and 14.5% for the 10 subblocks case. At the ends of the idealized crack, the crack opening is zero, yet the gradient of the opening is infinite. This large deviation at the crack ends results because the discretiza-

Table 2
Average error of the DDA program compared with experimental results by Grenoble [13]

Test No.	T1-5			T1-6			T1-7			T1-8			T1-9			T1-10		
H (cm)	80.52			97.28			115.7			134.37			151.38			227.2		
h (cm)	71.76			71.37			71.37			71.37			72.01			54.36		
Δh (cm)	8.76			25.91			44.33			63			79.37			172.84		
L (cm)	60.96			60.96			60.96			60.96			60.96			60.96		
$i(\Delta h/L)$	0.14			0.42			0.73			1.03			1.30			2.84		
Method	DDA	Lab	Error	DDA	Lab	Error	DDA	Lab	Error	DDA	Lab	Error	DDA	Lab	Error	DDA	Lab	Error
Port	h_d (cm)	h_l (cm)	E_i (%)	h_d (cm)	h_l (cm)	E_i (%)	h_d (cm)	h_l (cm)	E_i (%)	h_d (cm)	h_l(cm)	E_i (%)	h_d (cm)	h_l(cm)	E_i (%)	h_d (cm)	h_l (cm)	E_i (%)
1	79.93	79.88	−0.58	95.55	95.38	−0.69	112.60	112.65	0.11	130.18	130.56	0.60	146.35	147.45	1.38	215.75	217.81	1.19
2	79.96	79.88	−0.87	95.61	95.50	−0.39	112.70	113.16	1.03	130.28	131.19	1.45	146.30	147.70	1.76	216.00	218.57	1.48
3	79.17	79.25	0.87	93.27	93.47	0.78	108.71	109.22	1.15	124.64	126.37	2.74	139.01	142.49	4.38	200.18	201.93	1.01
4	80.01	79.88	−1.45	95.76	95.50	−0.98	112.90	112.52	−0.86	130.63	130.56	−0.12	146.61	146.94	0.42	216.89	217.04	0.09
5	80.04	80.01	−0.29	95.86	95.89	0.10	113.08	113.54	1.03	130.94	131.32	0.60	146.94	148.08	1.44	217.68	218.06	0.22
6	80.37	80.26	−1.16	96.82	96.77	−0.20	114.91	114.68	−0.52	133.22	133.10	−0.20	149.91	150.11	0.26	224.08	224.03	−0.03
7	78.84	78.99	1.74	92.30	92.84	2.06	107.11	108.20	2.46	122.22	124.84	4.15	136.42	140.97	5.73	194.06	200.79	3.89
8	78.89	78.99	1.16	92.46	92.96	1.96	107.32	108.46	2.58	122.61	125.10	3.95	136.86	141.35	5.66	195.07	201.17	3.53
9	75.64	74.80	−9.57	82.88	83.06	0.69	90.93	91.19	0.57	99.36	102.11	4.35	107.52	114.81	9.18	131.60	141.61	5.79
10	75.36	75.31	−0.58	82.02	81.92	−0.39	89.66	89.41	−0.57	97.31	98.55	1.98	105.31	111.00	7.17	125.98	133.86	4.56
11	75.97	75.95	−0.29	83.82	83.82	0.00	92.58	91.82	−1.72	101.68	103.51	2.90	110.49	116.33	7.36	138.00	144.40	3.70
12	76.73	76.96	2.61	86.13	87.00	3.33	96.70	97.79	2.46	107.26	111.38	6.53	117.45	125.60	10.27	153.09	165.10	6.95
13	76.86	76.96	1.16	86.46	87.38	3.53	97.31	98.68	3.09	108.08	112.40	6.85	118.41	127.00	10.82	155.17	167.39	7.07
14	76.40	76.45	0.58	85.12	85.60	1.86	94.87	95.63	1.72	104.78	107.32	4.03	114.20	120.90	8.45	146.53	157.99	6.63
15	76.61	76.58	−0.29	85.73	86.23	1.96	96.01	96.52	1.15	106.27	109.73	5.48	116.18	123.44	9.15	150.83	163.20	7.16
16	76.81	76.71	−1.16	86.39	86.61	0.88	97.03	97.28	0.57	107.80	110.36	4.07	118.57	123.95	6.78	154.41	163.96	5.53
17	73.05	72.77	−3.19	75.21	75.18	−0.10	77.90	77.72	−0.40	80.67	82.30	2.58	84.02	89.41	6.78	79.83	86.49	3.85
18	72.75	72.39	−4.06	74.30	74.42	0.49	76.53	76.45	−0.17	78.49	78.99	0.81	81.33	85.09	4.74	73.79	77.98	2.42
19	73.71	73.53	−2.03	77.17	77.47	1.18	81.23	81.79	1.26	85.42	88.65	5.12	90.22	96.14	7.46	92.91	100.46	4.36
20	73.13	72.90	−2.61	75.41	75.82	1.57	78.44	78.74	0.69	81.18	83.31	3.39	84.91	90.68	7.26	81.15	89.66	4.92
21	74.27	74.04	−2.61	78.82	78.99	0.69	83.97	84.33	0.80	89.43	92.96	5.60	95.30	100.46	6.50	103.99	113.67	5.60
22	72.85	72.52	−3.77	74.60	74.68	0.29	76.96	77.34	0.86	79.20	83.06	6.13	81.99	87.63	7.10	75.69	87.76	6.98
23	72.57	72.26	−3.48	73.74	73.91	0.69	75.39	75.82	0.97	77.11	79.50	3.79	79.35	83.82	5.63	70.05	78.11	4.66
24	72.29	71.88	−4.64	72.95	72.64	−1.18	74.14	74.17	0.06	75.21	77.09	2.98	76.99	80.39	4.29	64.82	71.63	3.94
E_h (%)		2.11			1.08			1.12			3.35			5.83			3.98	

tion of the crack is too coarse to account for the sharp curvature of the crack at its ends. Except for the crack ends, Fig. 10(a,b) indicate good agreement between the numerical and analytical predictions.

3.8. Effect of water level on tunnel stability

The excavation of a (half) circular tunnel is considered as a numerical example. The tunnel has a diameter, D, of 10 m and is located at a depth of 409.6 m below the surface. The water level varies between 100 and 500 m above the center of the tunnel. The domain of analysis is $5D$ (50 m) wide and $4D$ plus tunnel height (46.71 m) high. A vertical compressive stress of 10 MPa is applied on the top boundary of the domain (to simulate the load associated with 384.6 m of rock) and no lateral deformation is allowed. The intact rock has a unit weight of 26 KN/m^3, a Young's modulus of 3.6 GPa, and a Poisson's ratio of 0.2. The joints have a spacing of 4 m, a friction angle of 35°, and a cohesion of 0.5 MPa. No reinforcement is applied in this example. As boundary conditions, only elevation heads (zero pressure heads) were applied on the nodes along the excavated surface of the tunnel.

Without water the settlement of the tunnel roof was found to be equal to 165.2 mm (Table 3). The tunnel roof deforms but does not collapse as shown in Fig. 11(a). As the water level increases, the tunnel roof settlement increases resulting in complete collapse of the tunnel (see Table 3 and Fig. 11(b–f)).

4. Modeling sequential loading or unloading

4.1. Sequential excavation algorithm

A new algorithm to simulate sequential loading or unloading has been developed and implemented into

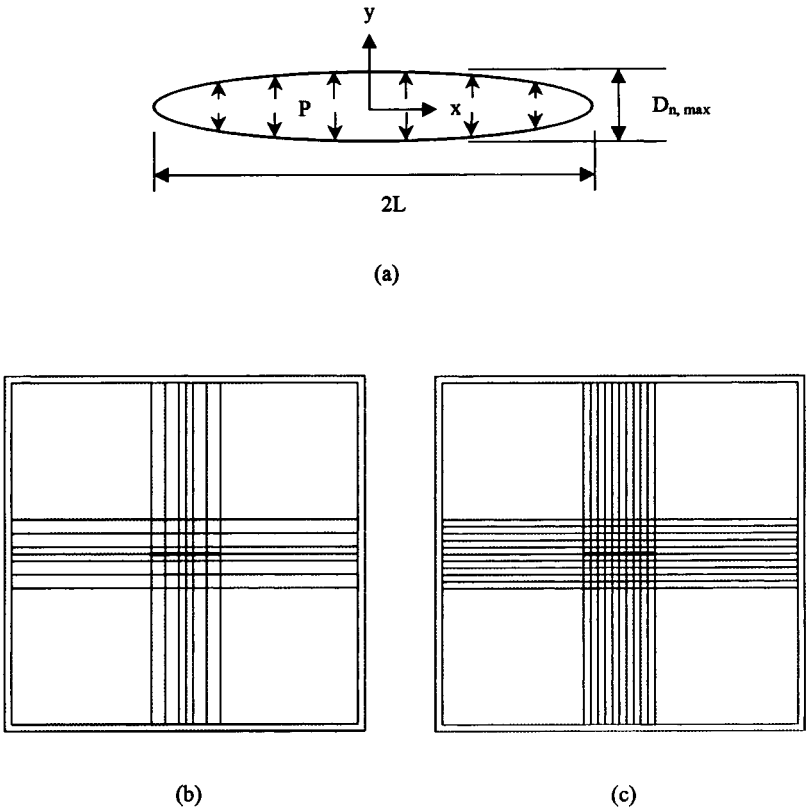

Fig. 9. Analysis of a pressurized crack in an infinite domain. (a) Representative section of a crack, (b) DDA model with crack walls divided into 6 subblocks, (c) DDA model with crack walls divided into 10 subblocks.

the DDA program. The algorithm can be used, for instance, to model the different phases of underground excavation. The algorithm consists of an iterative procedure where in situ stresses are first computed in all rock blocks before excavation. Then, the new stress distribution is determined following the first excavation step. The new stresses are then taken as initial stresses for the next excavation step. This iterative procedure continues until the end of the excavation process.

4.2. Analysis of excavation sequence of tunnels

As an example of application of the method, a rock mass 30 m wide and 20 m high consisting of 17 rock blocks is considered (Fig. 12). Three point loads are applied on block #15, to simulate structural loads at the ground surface. The intact rock has a unit weight of 23.6 kN/m^3, a Young's Modulus of 48 GPa, and a Poisson's ratio of 0.3. The joints have a friction angle of 40° and a cohesion of 4.0 MPa. No water flow was considered. Two sequences of excavation of a horseshoe tunnel in the rock mass of Fig. 12 were considered and are referred to as top-to-bottom and bottom-to-top. In the top-to-bottom (ex-t) excavation sequence, five blocks (numbered #32, #33, #31, #30, #29 in Fig. 12) were removed sequentially as shown in Fig. 13(b–f). In the bottom-to-top (ex-b) excavation sequence, five different blocks (numbered #29, #30, #31, #32, #33) were removed sequentially as shown in Fig. 14(b–f). The major principal stress σ_1 in blocks #18, #19, #23, #22 and #20 located on the left of the excavation surface was calculated for both excavation sequences. The results are plotted in Fig. 15(a,b,c,d,e).

Figure 15(a–e) indicate that the top-to-bottom excavation sequence induces much less stress concentration in the rock blocks adjacent to the excavated rock surface than the bottom-to-top excavation sequence. The results also show that in the bottom-to-top excavation sequence, the stress increases rapidly, which is more critical for the stability of the final excavated rock sur-

Table 3
Effect of water level on the stability of the tunnel in Fig. 11

Water level (m)	Roof settlement (mm)
0	165.2
100	237.6
200	706.4
300	1632.8
400	2088.2
500	4514.0

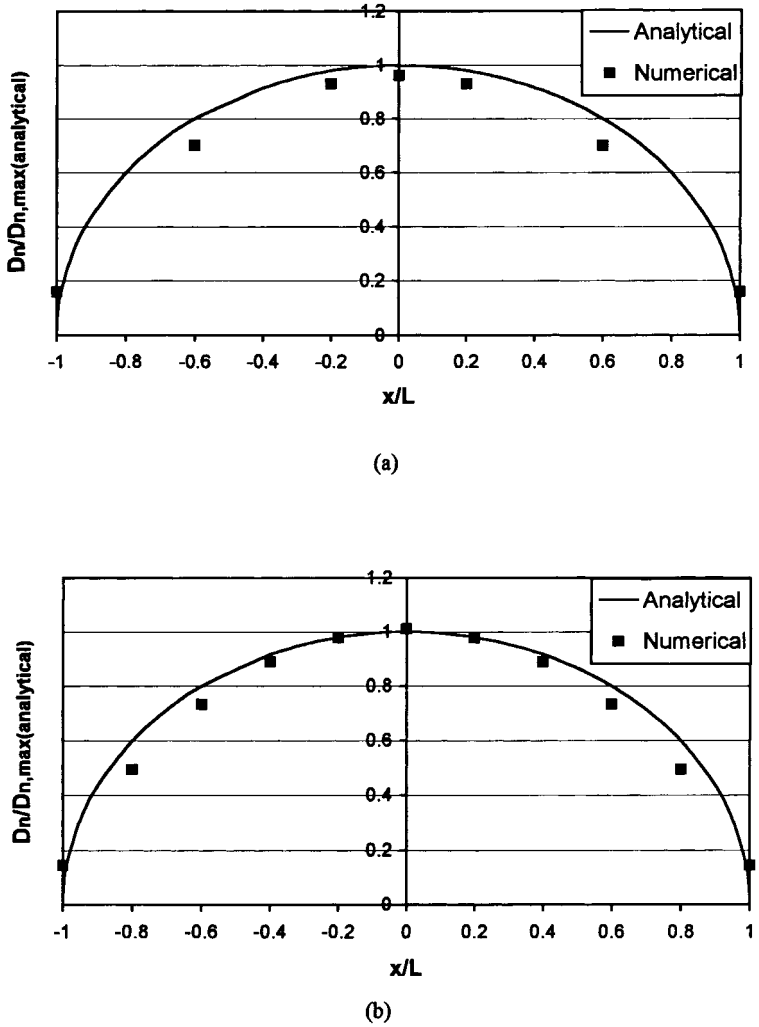

Fig. 10. Comparison between analytical and numerical solutions. (a) Case of 6 subblocks, (b) Case of 10 subblocks.

face. At the final excavation step (step 5), the top-to-bottom excavation sequence shows slightly smaller stresses than the bottom-to-top excavation sequence. These results indicate that the final stress distribution is influenced by the stress history induced by the excavation. This stress-path dependency is associated with geometrical nonlinearities in the DDA method as energy losses take place by friction along the joints and relative deformation of the blocks.

5. Modeling reinforcement by shotcrete and rockbolts

5.1. Shotcrete and concrete lining algorithm

A new algorithm to model shotcrete or concrete lining has been developed and implemented into the DDA program. The algorithm can be used to model the functions of shotcrete or concrete lining, i.e. sealing of rock surfaces, preserving inherent ground strength, and providing a structural arch. The algorithm creates shotcrete or concrete lining elements along the excavated rock surface with specified thickness and material properties, in order to simulate the application of shotcrete or the installation of concrete lining on already reinforced and excavated rock surfaces. After tunnel excavation, the geometrical data of the rock blocks along the excavated rock surface such as block numbers and nodal coordinates from the DDA program are used to compute block numbers and nodal coordinates of the shotcrete elements. The shotcrete elements are modeled as subblocks with specified thickness and material properties. The algorithm adds the shotcrete elements to existing rock blocks, thus changing the stiffness matrix of the blocky system. The initial stress in the shotcrete is assumed to be zero. As the rock blocks deform, the shotcrete elements are stressed. The new algorithm allows shotcrete elements

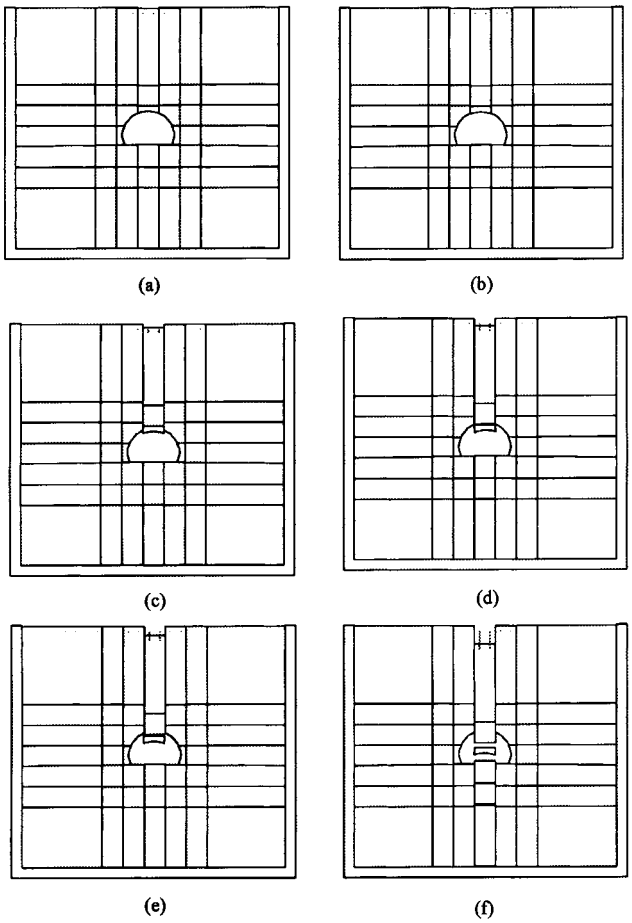

Fig. 11. Effect of water level on tunnel stability. (a) No water, (b) W.L.: 100 m, (c) W.L.: 200 m, (d) W.L.: 300 m, (e) W.L.: 400 m, (f) W.L.: 500 m.

to be installed step-by-step and therefore to simulate the construction sequence. In that case, the stresses in the shotcrete elements in a previous step are used as initial stresses for the next step, whereas the stresses in the newly installed shotcrete elements are assumed to be zero.

5.2. Rockbolt algorithm

The rockbolt algorithm suggested by Shi [1] was modified to be applicable to the case of sequential excavation and reinforcement, in which the axial force of a rockbolt at a previous step is applied as preloading in the next step. The algorithm applies a spring with specified stiffness between the starting and ending points of the rockbolt, thus changing the stiffness matrix of the blocky system. Consider a rockbolt connecting point P_1 (x_1, y_1) of block 1 and point P_2 (x_2, y_2) of block 2, which are not necessarily the vertices of the blocks as shown in Fig. 16(a). The length of the rockbolt is

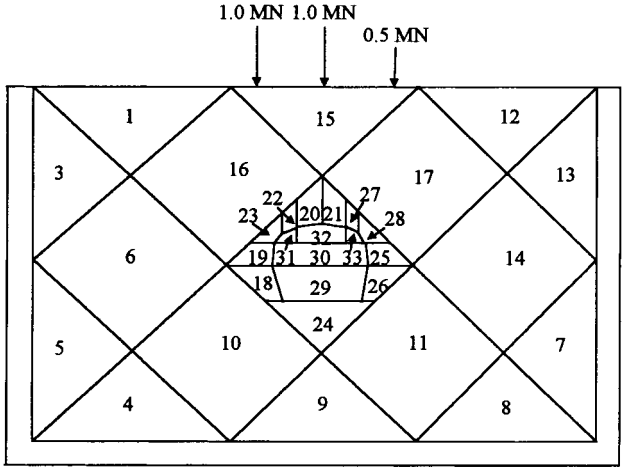

Fig. 12. Initial configuration for the analysis of sequential excavation of a tunnel.

$$l = \sqrt{(x_1 - x_2)^2 + (y_1 - y_2)^2} \tag{36}$$

The preloading of the rockbolt is assumed to be zero. As the rock blocks move as shown in Fig. 16(b), the rockbolt extends by an amount Δl equal to

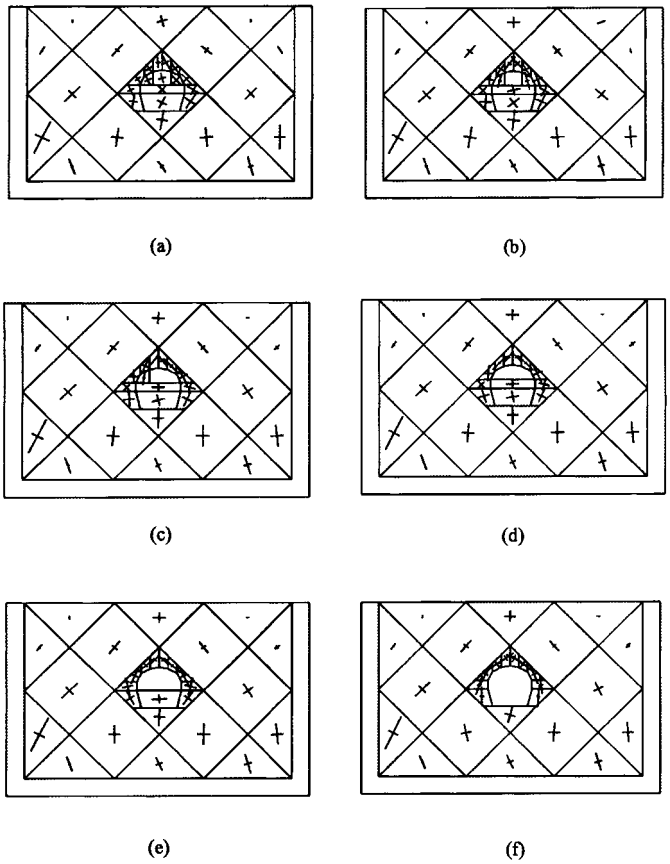

Fig. 13. Stress distribution for top-to-bottom excavation sequence. (a) Initial state (step 0), (b) step 1, (c) step 2, (d) step 3, (e) step 4, (f) step 5.

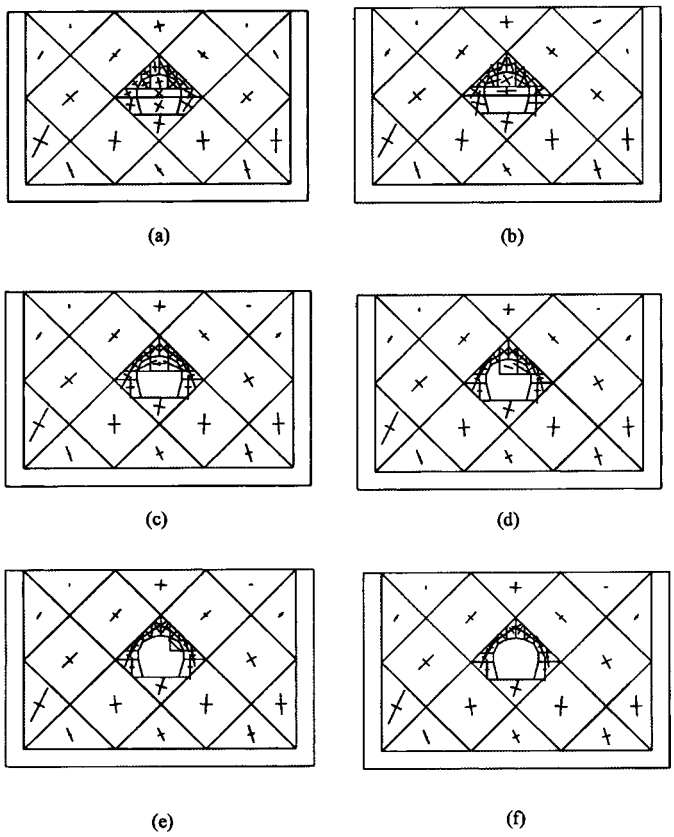

Fig. 14. Stress distribution for bottom-to-top excavation sequence. (a) Initial state (step 0), (b) step 1, (c) step 2, (d) step 3, (e) step 4, (f) step 5.

$$\Delta l = \left([D_i]^{\mathrm{T}} [T_i]^{\mathrm{T}} \begin{pmatrix} l_x \\ l_y \end{pmatrix} - [D_j]^{\mathrm{T}} [T_j]^{\mathrm{T}} \begin{pmatrix} l_x \\ l_y \end{pmatrix} \right), \tag{37}$$

where

$$l_x = \frac{1}{l}(x_1 - x_2) \quad l_y = \frac{1}{l}(y_1 - y_2) \tag{38}$$

are the direction cosines of the rockbolt. If s is the stiffness of the rockbolt, the axial force in the rockbolt is

$$F = -s\frac{\Delta l}{l} \tag{39}$$

The axial force in the rockbolt at a previous step is applied to the rockbolt as preloading in the next step as shown in Fig. 16(c).

The components F_x and F_y of the preloading force at point $P_1'(x_1', y_1')$ in block 1 are equal to

$$F_x = -F\, l_x \quad \text{and} \quad F_y = -F\, l_y \tag{40}$$

Likewise, the components F_x and F_y of the preloading force at point $P_2'(x_2', y_2')$ in block 2 are equal to

$$F_x = F\, l_x \quad \text{and} \quad F_y = F\, l_y \tag{41}$$

The preloading force at each point can be considered as point loading. For each block, the 6×1 submatrix for point loading is computed using Eqs. (29–32) and is added to the submatrix $\mathbf{F}_i$ in the global system of Eq. (4).

5.3. Effect of reinforcement on tunnel stability

The excavation and reinforcement by rockbolt of a (half) circular tunnel is considered as an example of application of the method. The tunnel has a diameter, D, of 10 m and is located at a depth of 409.6 m below the surface. The water level is 400 m above the center of the tunnel. The domain of analysis is $5D$ (50 m) wide and $4D$ plus tunnel height (46.71 m) high. A vertical compressive stress of 10 MPa is applied on the top boundary of the domain (to simulate the load associated with 384.6 m of rock) and no lateral deformation is allowed. The intact rock has a unit weight of 26 KN/m^3, a Young's modulus of 3.6 GPa, and a Poisson's ratio of 0.2. The joints have a spacing of 4 m, a friction angle of 35°, and a cohesion of 0.5 MPa. After excavation of the tunnel, two rockbolts (untensioned end-bearing type) were installed across the two vertical joints intersecting the tunnel roof. The stiffness of the rockbolts varies between 0 and 1×10^{12} N/m.

Without rockbolt reinforcement, the tunnel roof collapses as shown in Fig. 17(a) and the settlement of the

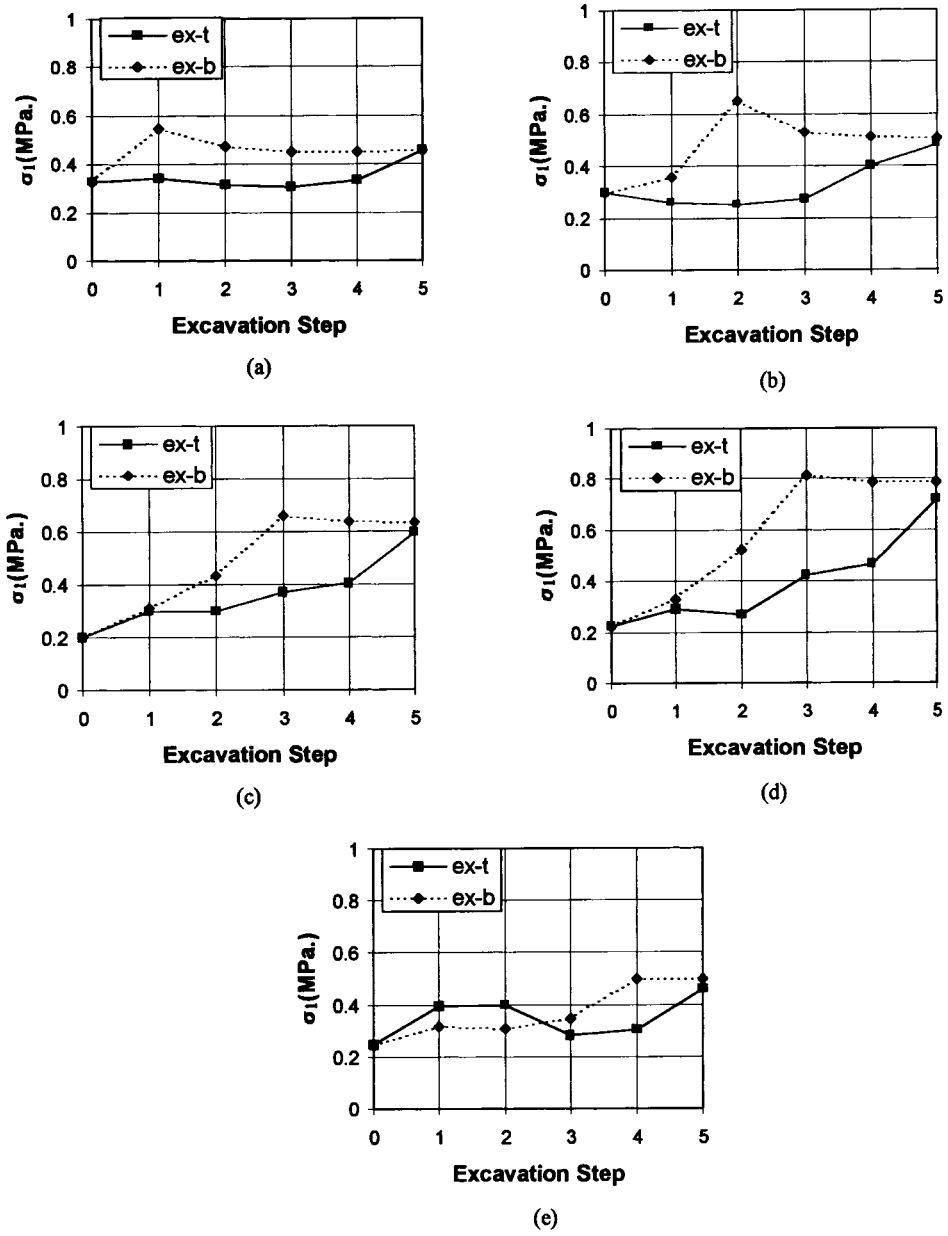

Fig. 15. Variation of σ_1 with step of excavation for the two excavation sequences of Figs. 13 and 14. (a) block #18, (b) block #19, (c) block #23, (d) block #22, (e) block #20.

tunnel roof was found to be equal to 1632.8 mm (Table 4). As the stiffness of the rockbolts increases, the tunnel roof settlement decreases (see Table 4 and Fig. 17(b,c,d,e,f)). Also, Table 4 indicates that the axial force in the rockbolts increases with the stiffness of the rockbolts.

6. Case study: modeling the excavation and reinforcement of the Unju tunnel

The Unju tunnel was selected as a case study (Daewoo Institute of Construction Technology [15]). The tunnel is located in Yeongigun Chungchungnamdo (Korea) and is part of the "Kyungbu High Speed Railway Project". Its depth ranges between 0 and 277.6 m (109K 820) and has a length of 4.02 km. A tunnel section (Station 109K 440) was selected for numerical analysis using our DDA program.

The half circular tunnel was excavated by the single bench cut method, and reinforced by shotcrete (thickness of 10 cm), rockbolts (diameter of 25 mm and length of 4 m) and concrete lining (thickness of 0.4 m). Rockbolts (untensioned end-bearing type) were installed along the upper half surface of the tunnel

Table 4
Effect of rockbolt stiffness on the stability of the tunnel in Fig. 17

Rockbolt Stiffness (N/m)	Rockbolt Axial force (N)	Roof settlement (mm)	Rockbolt reinforcement
0	0	1632.8	no
1×10^6	2.29×10^5	1204.1	yes
1×10^7	1.61×10^6	871.9	yes
1×10^9	3.39×10^7	286.6	yes
1×10^{11}	7.91×10^8	108.8	yes
1×10^{12}	1.20×10^9	69.3	yes

only. The spacing of the rockbolts was 2 m longitudinally and 11.3° latitudinally (with a total number of 15). The ground condition above the tunnel is represented in Fig. 18. The radius of the excavation is 7.6 m (tunnel radius = 7.1 m, shotcrete thickness = 0.1 m, lining thickness = 0.4 m). The geology of the station consists of augen and banded gneiss. From the geological site investigation report, the ground above the tunnel is mostly hard rock with a very small depth of weathered rock and soft rock. The intact rock has a unit weight of 26 kN/m^3, a Young's modulus of 3.6 GPa, and a Poisson's ratio of 0.2. The joints have a friction angle of 33.5° and a cohesion of 0.11 MPa. The shotcrete has a unit weight of 23 kN/m^3, a Young's modulus of 15 GPa, and a Poisson's ratio of 0.25. The Young's modulus of the rockbolts is 214 GPa. The domain of analysis was set as $5D$ horizontally and $4D$ (plus tunnel height) vertically, where D is the tunnel diameter equal to 15.2 m. A vertical compressive stress of 4.83 MPa was applied on the top boundary of the domain (to simulate the load associated with 185.7 m of rock).

The joint location and orientation data for station 109K 440 used in the DDA analysis were obtained

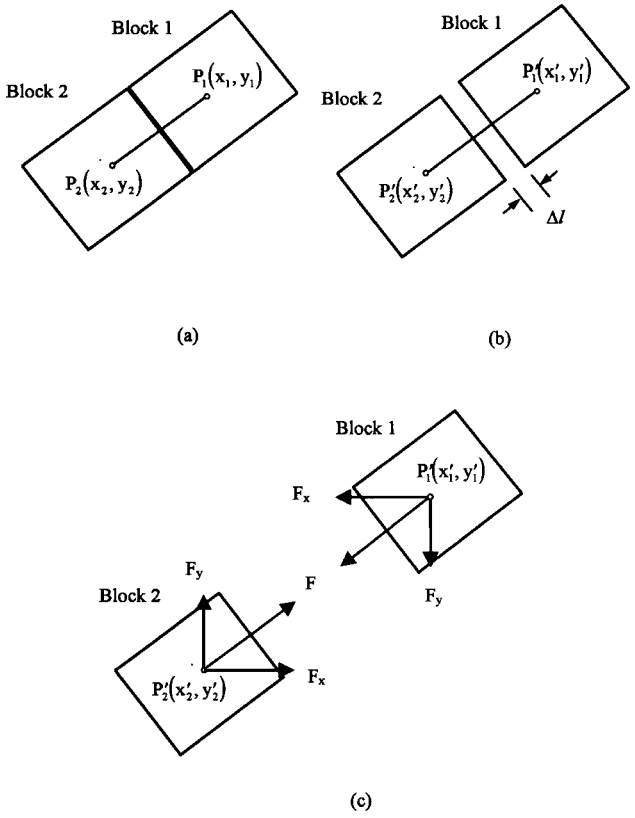

Fig. 16. Computation of rockbolt preloading. (a) Initial state, (b) Deformed state, (c) Conversion of axial force of rockbolt as preloading in next step.

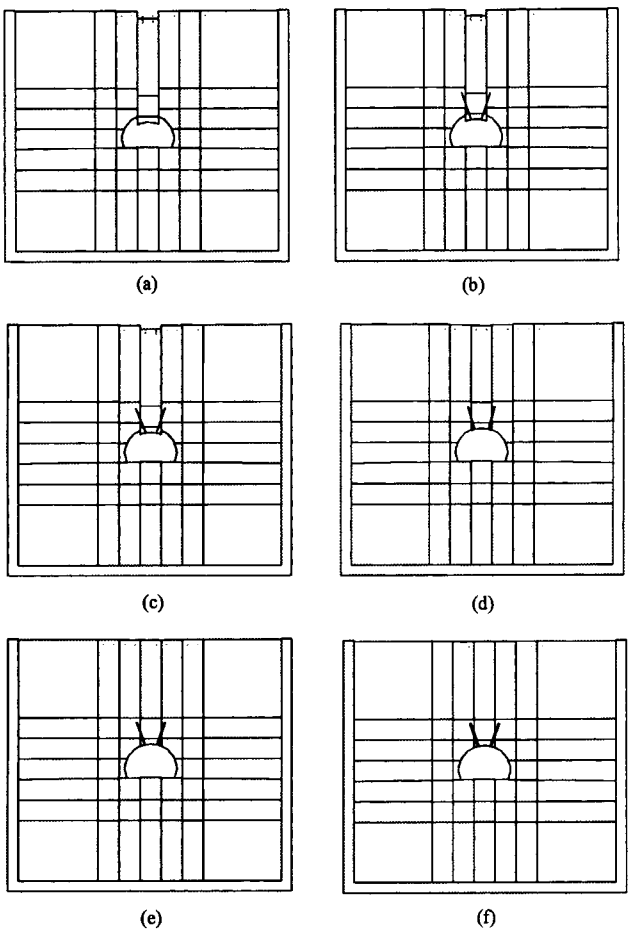

Fig. 17. Effect of rockbolt on tunnel stability for different values of rockbolt stiffness. (a) No rockbolt, (b) stiffness: 1×10^6 N/m, (c) stiffness: 1×10^7 N/m, (d) stiffness: 1×10^9 N/m, (e) stiffness: 1×10^{11} N/m, (f) stiffness: 1×10^{12} N/m.

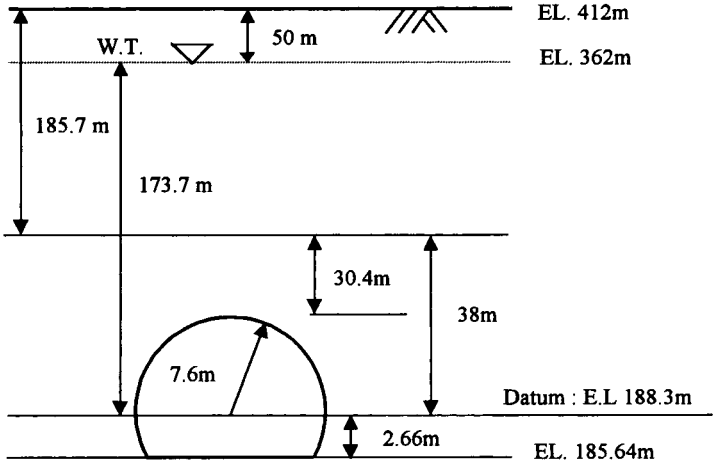

Fig. 18. Ground condition of the Unju tunnel (station 109K 440).

from tunnel face mapping photographs at Station 109K 442 located near the station of interest. The joints were assumed to be continuous and to extend over the entire domain of analysis. The initial geometry is shown in Fig. 19(a). Construction (excavation and reinforcement) of the tunnel was conducted in five steps outlined in Table 5. These five steps were simulated using our DDA program. The stress distribution at the end of each step is shown in Fig. 19(b–f).

The tunnel roof settlement, the axial force in the 15 rockbolts, and the tangential stresses in the shotcrete segments were predicted using the DDA analysis and compared with actual field measurements. The computed and measured data are listed in Table 6. These results indicate that rockbolts #7 and #10, which intersect natural rock joints, develop large tensile forces (42 and 81 kN). This observation shows the effectiveness of rockbolt reinforcement in preventing relative movement between blocks in a rock mass. The stresses in the shotcrete show small compression. The results in Table 6 indicate that rockbolts act as a major reinforcement of rock blocks and shotcrete functions as auxiliary reinforcement such as sealing of rock surface, preserving inherent ground strength and providing a structural arch.

7. Conclusion

Three major extensions were implemented into the original DDA program of Shi [1] and modified by Lin [8]. The extensions include hydro-mechanical coupling between rock blocks and water flow in fractures, sequential loading and unloading, and rock reinforcement by shotcrete, rockbolt and concrete lining.

The hydro-mechanical coupling algorithm is very important in rock engineering problems where seepage takes place in natural fractures and joints. Seepage forces and water pressure can be controlling factors in rock mass stability as illustrated in the tunnel example presented in this paper. The new algorithm is limited to two-dimensional steady state flow and needs to be modified to include transient flow phenomena.

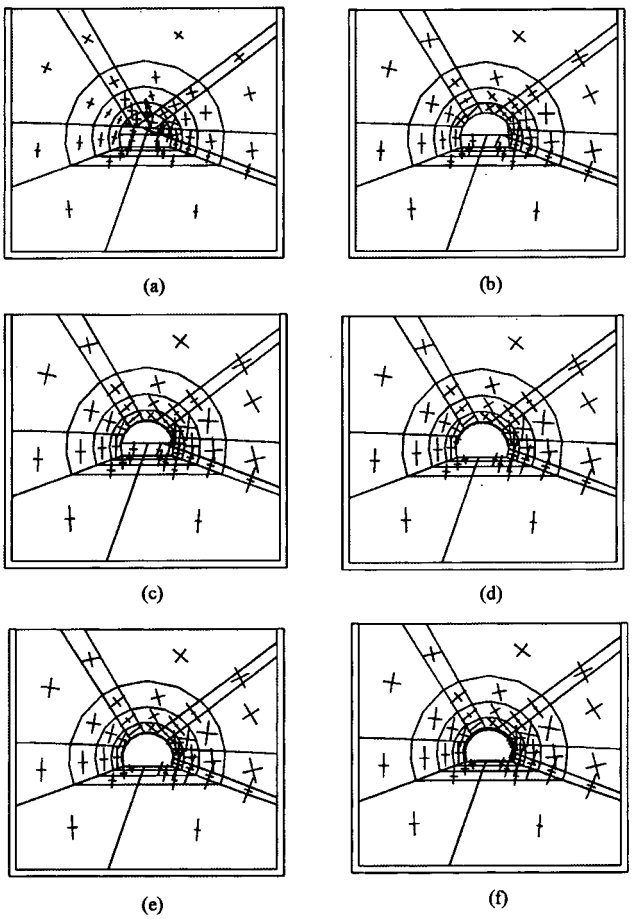

Fig. 19. Construction sequence of the Unju tunnel (109K 440). (a) Step 0, (b) step 1, (c) step 2, (d) step 3, (e) step 4, (f) step 5.

Table 5
Steps of excavation and reinforcement for the Unju tunnel

Step	Contents
0	Initial state without excavation
1	Excavation of upper half section
2	Reinforcement of the upper half section with shotcrete and rockbolts
3	Excavation of lower half section
4	Reinforcement of lower half section with shotcrete
5	Reinforcement of full section with concrete lining

Table 6
Comparison between computed and measured data (Unju tunnel)

Item	DDA	Measured data	App.
Roof settlement (mm)	4.3	4	+: Down, −: Up
Rock bolt axial force (kN)	−3.97 (1)	−3.88 (1)	−: Compression, +: Extension
	−0.70 (2)		
	4.82 (3)		
	3.03 (4)		
	−0.85 (5)		
	0.93 (6)		
	41.98 (7)		
	−0.51 (8)	−0.20 (8)	
	9.68 (9)		
	80.74 (10)		
	6.07 (11)		
	7.01 (12)		
	−4.86 (13)		
	−4.58 (14)	−4.08 (14)	
	2.87 (15)		
Tangential shotcrete stress (MPa)	−0.007 (a)		
	−0.013 (b)	−0.014 (b)	
	−0.015 (c)		
	−0.015 (d)		
	−0.013 (e)	−0.012 (e)	
	−0.035 (f)		
	−0.035 (g)		
	−0.036 (h)		
	−0.026 (i)		
	−0.009 (j)	−0.011 (j)	

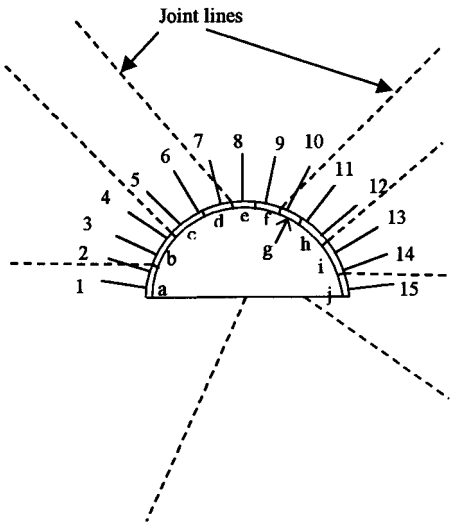

The sequential loading (or unloading) algorithm allows for changes in loading conditions that can occur in rock engineering problems. In the examples presented herein, the changes were associated with the excavation of underground openings. The same algorithm could also be used to model surface excavations associated with road cuts, open pit mining, quarrying, etc. It is likely that the overall final stability of a rock mass depends on the excavation sequence and the corresponding stress history. This interesting phenomenon can now be studied and researched using our new DDA program.

The shotcrete or concrete lining algorithm creates shotcrete or concrete lining elements along the excavated rock surface with specified thickness and material properties, which simulates applying shotcrete or installing concrete lining on already reinforced and excavated rock surfaces. The rockbolt algorithm suggested by Shi [1] was modified to be applicable to the cases of sequential excavation and reinforcement, in which axial forces of rockbolts at a previous step are applied to the rockbolts as preloading in the next step.

The DDA program with the three new extensions can now be used as a practical tool in the design of underground structures such as tunnels or caverns. It can also be used to analyze the stability of concrete dams on fractured rock masses. The main contribution

of this paper is that phases of construction (excavation, reinforcement) can now be simulated in a more realistic way. It is noteworthy that the method presented in this paper is limited to solving two-dimensional problems.

Acknowledgements

The support of Daewoo Corporation (Construction Division) is gratefully acknowledged.

References

[1] Shi GH. Discontinuous deformation analysis: a new numerical model for the statics and dynamics of block systems. Ph.D. thesis, University of California, Berkeley, CA, 1988.
[2] Shi GH, Goodman RE. Generalization of two-dimensional discontinuous deformation analysis for forward modeling. International Journal for Numerical and Analytical Methods in Geomechanics 1989;13:359–80.
[3] Shi GH. Forward and backward discontinuous deformation analyses of rock systems. In: Proceedings of International Conference of Rock Joints. Norway: Leon, 1990. p. 731–43.
[4] Ke TC, Goodman RE. Discontinuous deformation analysis and 'the artificial joint concept'. In: Proceedings of 1st NARMS, UT, Austin, 1994. p. 599–606.
[5] Yeung MR, Klein SJ. Application of the discontinuous deformation analysis to the evaluation of rock reinforcement for tunnel stabilization. In: Proceedings of 1st NARMS, UT, Austin, 1994. p. 607–14.
[6] Salami MR, Banks D. Discontinuous deformation analysis (DDA) and simulations of discontinuous media. In: Proc. of the First International Forum on Discontinuous Deformation Analysis (DDA) and Simulations of Discontinuous Media, Berkeley, CA, 1996.
[7] Ohnishi Y. Proc. of the Second International Conference on Analysis of Discontinuous Deformation, Kyoto, Japan, 1997.
[8] Lin CT. Extensions to the discontinuous deformation analysis for jointed rock masses and other block systems. Ph.D. thesis, University of Colorado at Boulder, CO, 1995.
[9] Szechy K. The Art of Tunnelling. Budapest: Akademiai Kiado, 1967.
[10] Louis C. A study of groundwater flow in jointed rock and its influence on the stability of rock masses. Imperial College, Rock Mechanics Research Report No. 10, 1969.
[11] Asgian MI. A numerical study of fluid flow in deformable, naturally fractured reservoirs. Ph.D. thesis, University of Minnesota, MN, 1988.
[12] Amadei B, Carlier JF, Illangasekare TH. Effects of turbulence on fracture flow and advective transport of solutes. Int J Rock Mech Min Sci Geomech Abs 1995;32:343–56.
[13] Grenoble BA. Influence of geology on seepage and uplift in concrete gravity dam foundations. Ph.D. thesis, University of Colorado at Boulder, CO, 1989.
[14] Sneddon IN, Lowengrub M. Crack problems in the classical theory of elasticity. New York: John Wiley and Sons, Inc, 1969.
[15] Daewoo Institute of Construction Technology. Final report on instrumentation of UNJU tunnel – Kyungbu High Speed Rail Way Project 4-3 Section. Suwon, Korea: Deawoo Co. (Construction Division), 1995.